

Strong Reduction of Thermal Conductivity of WSe₂ with Introduction of Atomic Defects

Bowen Wang^a, Xuefei Yan^a, Hejin Yan^a, Yongqing Cai^{a*}

^aInstitute of Applied Physics and Materials Engineering, University of Macau, Macau, China

Abstract

The thermal conductivities of pristine and defective tungsten diselenide (WSe₂) are investigated by using equilibrium molecular dynamics method. The thermal conductivity of WSe₂ increases dramatically with size below a characteristic width of ~5 nm and levels off for broader samples and reaches a constant value of ~2 W/mK. By introducing atomic vacancies, we discovered that the thermal conductivity of WSe₂ is significantly reduced. In particular, the W vacancy has a greater impact on thermal conductivity reduction than Se vacancies: the thermal conductivity of pristine WSe₂ reduced by ~60% and ~70% with the adding of ~1% of Se and W vacancies, respectively. The reduction of thermal conductivity is found to be related with the decrease of mean free path (MFP) of phonons in the defective WSe₂. The MFP of WSe₂ decreases from ~4.2 nm for perfect WSe₂ to ~2.2 nm with the adding of 0.9% Se vacancies. More sophisticated types of point defects, such as vacancy clusters and anti-site defects, are

explored in addition to single vacancies, and are found to dramatically renormalize the phonons. The reconstruction of the bonds leads to localized phonons in the forbidden gap in the phonon density of states which leads to the drop of thermal conduction. This work demonstrates the influence of different defects on thermal conductivity of single-layer WSe₂, providing insight into the process of defect-induced phonon transport as well as ways to improve heat dissipation in WSe₂-based electronic devices.

Keywords: molecular dynamics, thermal conductivity, WSe₂, atomic defects, phonon,

1. INTRODUCTION

Due to its extraordinary properties[1-3], two-dimensional (2D) transition metal dichalcogenides (TMDs) with sandwich structures have piqued researchers' attention in a variety of fields, including electronics[4-8], optoelectronics[9-11], and thermoelectrics [12-16]. Semiconducting tungsten diselenide (WSe₂), one of the TMDs, drawn a lot of interest for thermal management of device due to its ultra-low thermal conductivity[17]. Experimental measurements[18-20] and numerical simulations[21-23] have both applied to explore inherent thermal properties of single-layer WSe₂. WSe₂ thin films have an in-plane thermal conductivity of around 1.5 W/mK measured by using a suspended device[24]. To comprehensively study the lattice thermal conductivity of WSe₂ monolayers, Zhou et al. employed first-principles calculations paired with the phonon Boltzmann transport equation[25], and discovered that the single-layer WSe₂ have extremely low thermal conductivity (3.935 W/mK) due to its ultralow Debye

frequency and hefty atom mass. Because of its low heat conductivity and direct bandgap semiconducting nature, WSe₂ is an attractive candidate for thermoelectric applications.

According to earlier studies[26-30], different types of defects have a considerable impact on mechanical, electrical, and thermal properties. Meanwhile, structural defects were unavoidable and discovered in as-grown 2D materials due to growth and integration[31-33]. In the as-grown single-layer WSe₂, for example, structural defects such as point defects are ubiquitous[34, 35]. It is thus critically important to investigate the impact and mechanisms of defects and their impact on WSe₂, which is crucial for thermal management in WSe₂-based thermoelectric applications. The thermal conductivity of amorphous WSe₂ thin films in cross-plane was measured experimentally by Chiritescu et al. to be as low as 0.05 W/mK at ambient temperature due to extensive phonon localization[18]. Disordered WSe₂ has a thermal conductivity significantly lower than compacted single-crystal platelets, according to Shi et. al[36]. Previous calculations on the thermal properties of WSe₂ were confined to pristine WSe₂ configurations[23, 37], despite extensive simulations on defective materials were reported such as graphene[38] and MoSe₂[39]. Overall, despite previous research showing that the presence of lattice defects reduces thermal transport characteristics, only a few research have looked into how defects affect thermal transport in single-layer WSe₂ and the phonon transport mechanism of defective WSe₂ is missing.

In this work, the effects of size and various defects on thermal properties of WSe₂ are explored using equilibrium molecular dynamics (EMD) simulations. The mean free

path (MFP) of phonons is extrapolated to illustrate the reduction of thermal conductivity explained by the undercoordinated atoms near the vacancies. The formation energies of higher order defects are calculated and their impact on the thermal conductivity of WSe₂ are also studied. By examining phonon density of states (PDOS), physical process of thermal conductivity lowering with different defects was investigated.

2. METHODOLOGY

The large-scale atomic/molecular massively parallel simulator (LAMMPS)[40] was used to run all of our molecular dynamics (MD) simulations in this investigation. We employ the Stillinger-Weber (SW) reported by Norouzzadeh et. al[23] to describe interatomic interactions, which reproduces the phonon dispersion in close to first-principles calculations[41] and obtain in-plane thermal conductivity results fitting well with experiments[25]. The formation energies of point defects seen in single-layer WSe₂ that we obtained from this potential accord well with DFT simulations on a quantitative level[42]. The Fig. 1 illustrates the hexagonal sandwiched form of the WSe₂ structure from the top and side. In the x (zigzag) and y (armchair) directions, the periodic boundary condition was utilized, whereas the free boundary condition was used in the z direction. Each structure is initially equilibrated for 100000 time steps at constant volume and 300 K using a time step of 0.5 fs. After the equilibration, we proceed with

a constant energy run NVE for up to 1×10^8 time steps. To make a more consistent analysis, for each content of defect, five independent configurations with different length and randomly produced defective configurations are calculated and the values are averaged. It was reported[43] that that in single-layer WSe₂, in-plane thermal conductivity in the armchair direction is kind of stronger than in the zigzag direction, and this anisotropy being more prominent at low temperatures. In this work, by using EMD method, we mainly focus on the thermal conductivity along the armchair directions at 300 K. The principles of fluctuation dissipation and linear response[44] are utilized to compute thermal conductivity within the EMD paradigm[45]. The heat flux vectors, as well as their correlations, are computed during the simulation. The thermal conductivity in the armchair direction κ_{yy} , is connected to the heat current autocorrelation function (HCACF) by Green-Kubo expression[44, 46]

$$\kappa_{yy} = \frac{1}{Vk_B T^2} \int_0^\tau \langle j_y(t) \cdot j_y(0) dt \rangle, \quad (1)$$

where the V , k_B , T represent system volume, Boltzmann constant, system temperature respectively. The angular brackets indicate an ensemble average of the heat flux j auto-correlation.

We calculate the PDOS of WSe₂ with different vacancy configurations by taking the Fourier transform of the velocity autocorrelation function in order to depict the phonon vibrations at different frequencies:

$$F(\omega) = \frac{1}{\sqrt{2\pi}} \int_{-\infty}^{\infty} e^{-i\omega t} \langle v(t) \cdot v(0) \rangle / (\langle v(0) \rangle \cdot v(0)) dt, \quad (2)$$

where $F(\omega)$ represents the PDOS at ω angular frequency, $v(t)$ and $v(0)$ represent the atomic velocity vectors at the time of t and 0, respectively.

3. RESULTS AND DISCUSSION

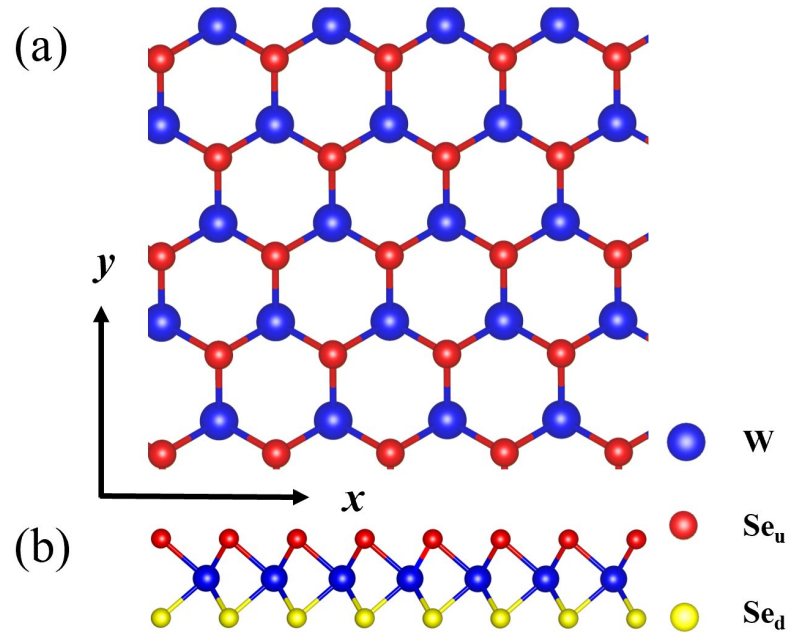


Figure 1. Top and side views of single-layer WSe₂ configuration. The top and bottom layers' selenide atoms are shown by red and yellow balls, respectively and the blue balls represent tungsten atoms.

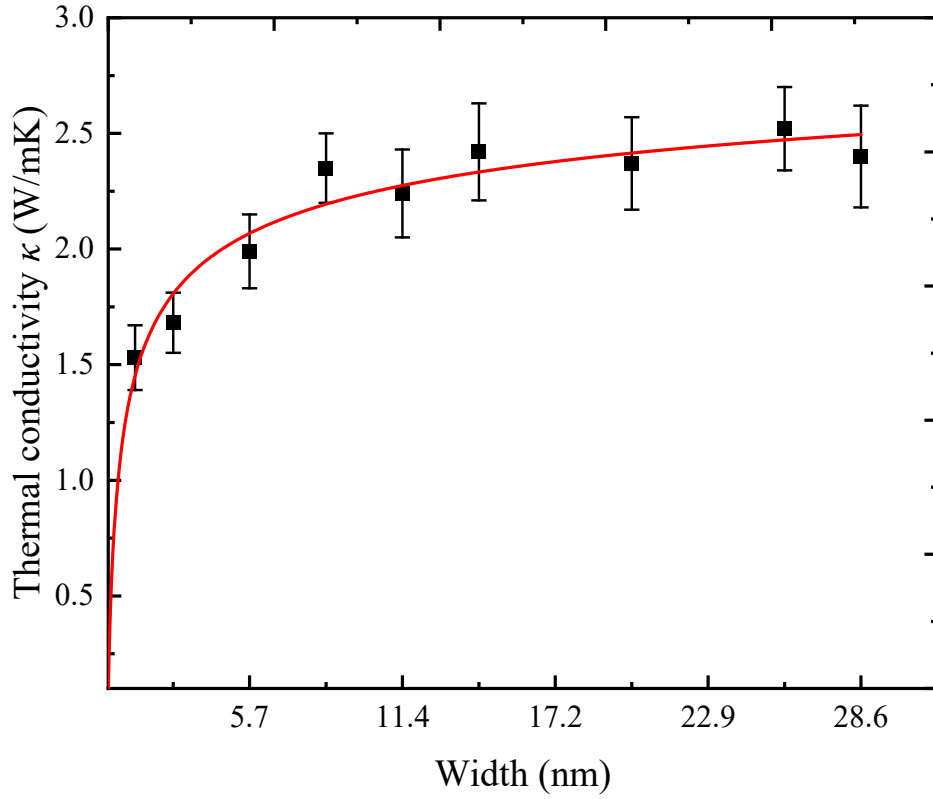


Figure 2. Thermal conductivity as a function of width for thermal conductivity in the armchair direction with a length of 50 nm. The point corresponds to the data points while the solid line represents the fitted curve.

Firstly, the effect of width (normal to the transport direction) of the model on thermal conductivity is examined. The length of all simulated single-layer WSe₂ was fixed to 50 nm which is wide enough to resolve the Brillion zone while also avoiding a thermal conductivity forecast divergence. Fig.2 depicts the width dependence of thermal conductivity for single-layer WSe₂ with considering width ranging from 3 to 28.6 nm. To suppress the uncertainty arisen from the statistical thermal fluctuations which are likely to occur in the calculation of thermal conductivity using molecular dynamics[47], 10 independent simulations for various cell widths are performed. We can observe that

when the width rises, the thermal conductivity increases as well. The thermal conductivity of WSe₂ increases dramatically with size below a characteristic width of ~ 5 nm and levels off for broader samples and reaches a constant value of ~ 2 W/mK. The thermal transport here is governed by Umklapp scattering and boundary scattering, and the latter is more dominant than Umklapp scattering when the width is narrow. The thermal conductivity of WSe₂ increases as the width grows due to a reduction in scattering from the edge localized phonon effect. The Umklapp scattering becomes the leading factor that governs the phonon scattering while the boundary scattering becomes gradually weakened.

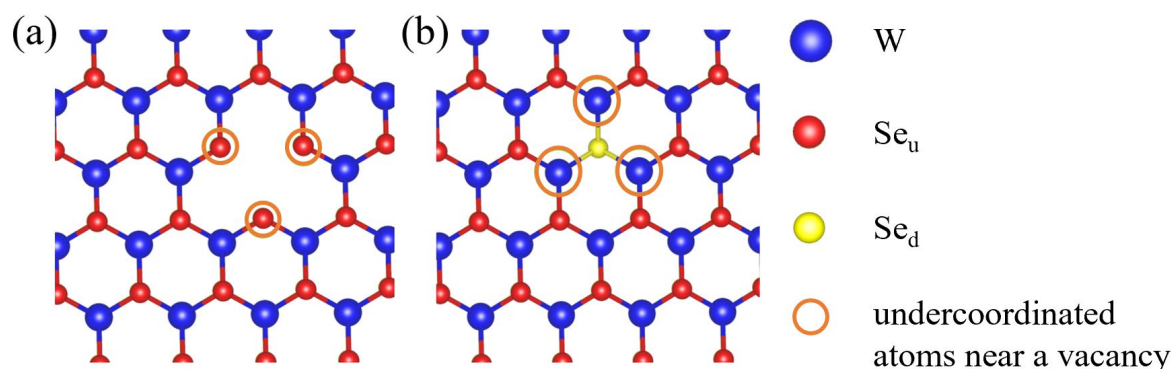


Figure 3. Atomic configurations for single tungsten vacancy (a) and selenium vacancy (b) in single-layer WSe₂.

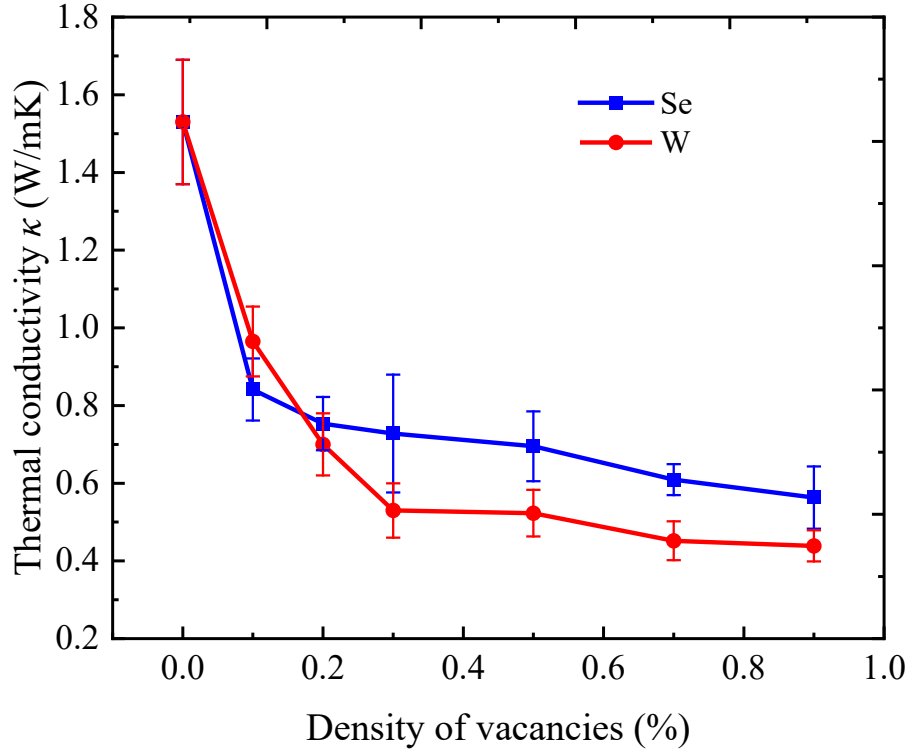
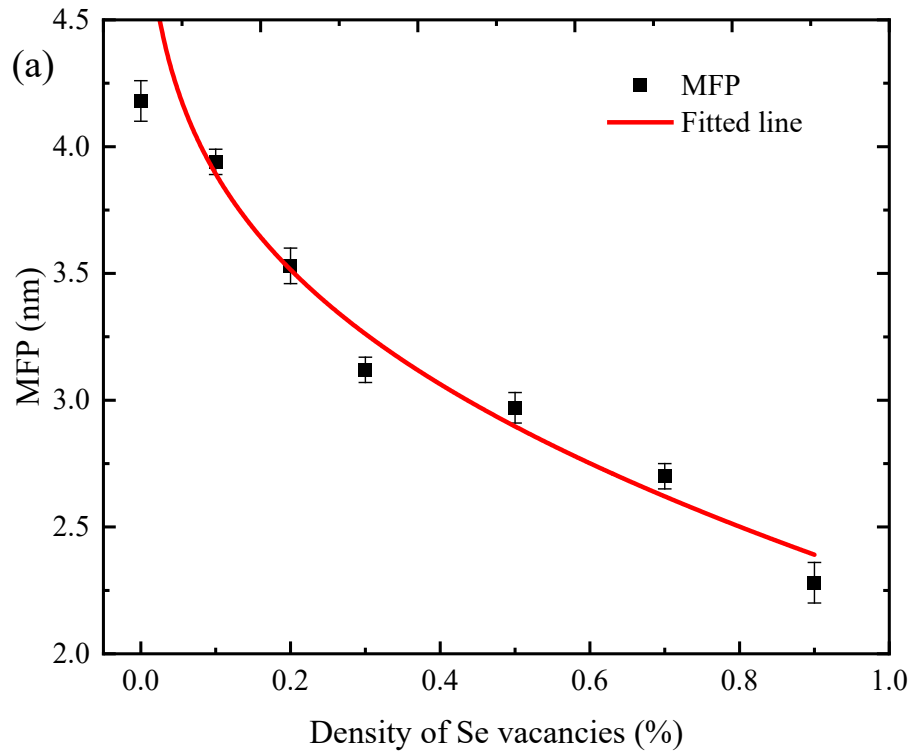


Figure 4. Thermal conductivity of single-layer WSe₂ in relation to defect ratio of W and Se vacancies.

To see how defects affect phonon transport in WSe₂ monolayers, the in-plane size of the simulation box is fixed as 50×10 nm and five independent simulations with randomly produced vacancies are carried for a specific content of vacancy. Both of the thermal conductivity of pristine single-layer WSe₂ (1.53 ± 0.16 W/mK) calculated by EMD method and MFP extrapolated (4.18 ± 0.08 nm) fits well with NEMD results reported by Norouzzadeh[23]. Trends in thermal conductivity with two different vacancies: Se vacancy (V_{Se}) and W vacancy (V_W), are shown in Fig. 4. The thermal conductivity of pristine WSe₂ fell sharply as the defect concentration rises from 0% to

0.9% and reduced by $\sim 60\%$ and $\sim 70\%$ when the density of vacancies equal to 0.9% for V_{Se} and V_{W} , respectively. The significant influence of defects on thermal conductivity is also found in MoS_2 [48] and MoSe_2 [49]. The V_{W} has a greater impact on the thermal conductivity of WSe_2 , similar to the case of MoS_2 with lattice defects [50]. Reduction of relaxation time (τ) and mean free path (MFP), which caused by missing atoms, linkages, and different force constants near vacancies, are the main causes of thermal conductivity reduction.



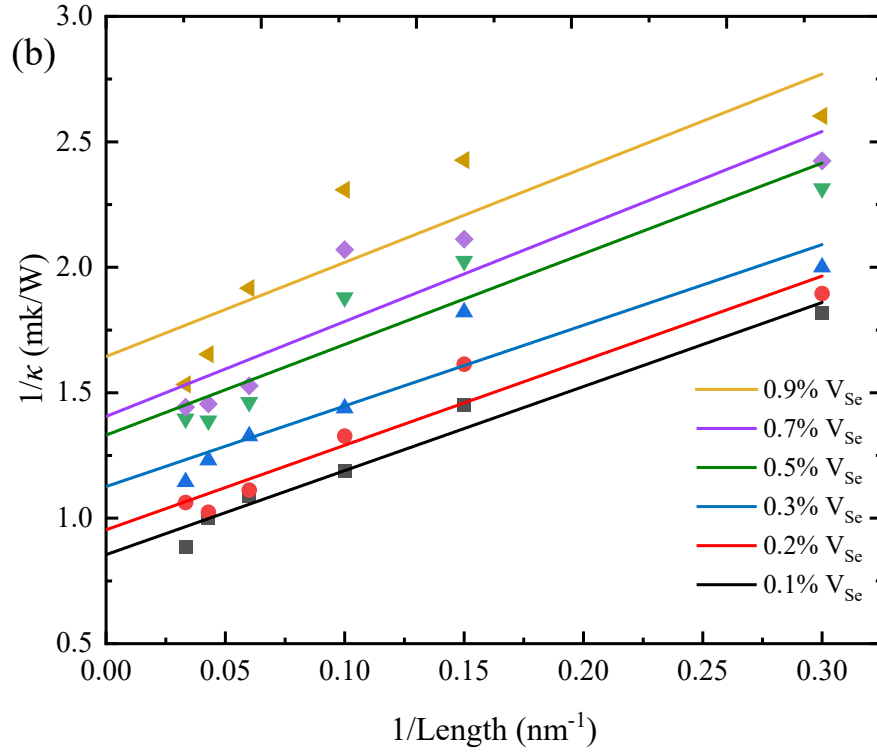


Figure 5. (a) Mean free path of WSe₂ in relation to density of V_{Se} at 300 K. (b) The inverse of thermal conductivity versus inverse of length in WSe₂ containing different contents of V_{Se}.

The following formula relates the thermal conductivity of a single layer material with a limited length to the thermal conductivity of an endlessly long single-layer [51]:

$$\frac{1}{\kappa} = \frac{1}{\kappa_{\infty}} \left(\frac{1}{L} + 1 \right) \quad (3)$$

Where L is the phono MFP. The thermal conductivity of finite length and infinitely long single-layer are represented by κ , κ_{∞} , respectively. As a result, single-layer thermal conductivity's inverse is proportional to the inverse of their lengths. The MFP of

defective single-layer WSe₂ is extrapolated in Fig. 5(a) and Fig. 5(b) illustrates the inverse of thermal conductivity versus inverse of single-layer lengths. Here we only examine V_{Se} which is more likely to be formed owing to a lower formation energy than V_W as we will show below. The MFP of WSe₂ is found to decrease from ~4.2 nm for perfect WSe₂ to ~2.2 nm with the adding of Se vacancy at 0.9% V_{Se}. Because the MFP of a phonon is inversely related to its scattering rate, a smaller MFP indicates an increase in scattering rate and a drop in heat conductivity.

Matthiessen's rule[52] states that the total scattering rate τ^{-1} is written as:

$$\tau^{-1} = \tau_{Anh}^{-1} + \tau_B^{-1} + \tau_V^{-1} + \tau_F^{-1} \quad (4)$$

where τ_{Anh}^{-1} and τ_B^{-1} represent the Umklapp phonon-phonon and phonon-boundary scattering rate respectively, τ_V^{-1} is related to loss of atom near the vacancy, and τ_F^{-1} is induced by the shift in force constants between the undercoordinated atoms near the vacancies. τ_V^{-1} can be written as[53, 54]:

$$\tau_V^{-1} = x \left(-\frac{M_V}{M} - 2 \right)^2 \frac{\pi}{2} \frac{g(\omega) \omega^2}{N} \quad (5)$$

where x is the defect concentration, M is the atomic mass average, M_V is the absent atom's mass at the void, $g(\omega)$ is the phonon DOS and N is atoms number.

According Eq. 5, τ_V^{-1} induced by V_W is greater than that by V_{Se} since the atomic masses of the W (183.84) is significantly high than Se (78.971) atoms. This is true in the sense in Fig. 4 that V_W affects thermal conductivity more than V_{Se} as the variation

in $g(\omega)$ and G caused by vacancies are small because of the small concentrations of vacancies in our study.

τ_F^{-1} can be written as:

$$\tau_F^{-1} = nx\left(\frac{\delta k}{k}\right)^2 4\pi \frac{\omega^2 g(\omega)}{G} \quad (6)$$

where n is the number of atoms located around the vacancy, x and δk are force constants before and after the change. For single V_{Se} and single V_W , n equals 3 and 6, respectively, as illustrated in Fig. 3. The δk caused by the V_W is bigger than that caused by the V_{Se} due to higher atomic mass of W. According to Eq. 6, the scattering rate induced by variation of force constants around vacancies τ_F^{-1} is greater induced by the V_W .

In addition to the V_{Se} and V_W single-vacancy-type defects, we also calculate other types of vacancies which are possible in the WSe_2 . Zhang et. al[34] found that the W related defects are likely to occur and three possible defect structures are proposed including the anti-site of W and Se atom (Se_W) in which a Se atom replaces a W atom, vacancy complex of three missing Se atoms near the W vacancy site (V_{WSe3}) and vacancy complex of three missing Se atoms near the W atom (V_{Se3}). Besides, other types of vacancies: the two Se vacancies in an apical form (V_{Se2}) and the six vacancies arranged in chain (V_{Se6C}) and triangle (V_{Se6T}) forms. The latter configurations were observed in WS_2 by using scanning transmission electron microscopy[31]. The vacancy structures are shown in Fig. 6.

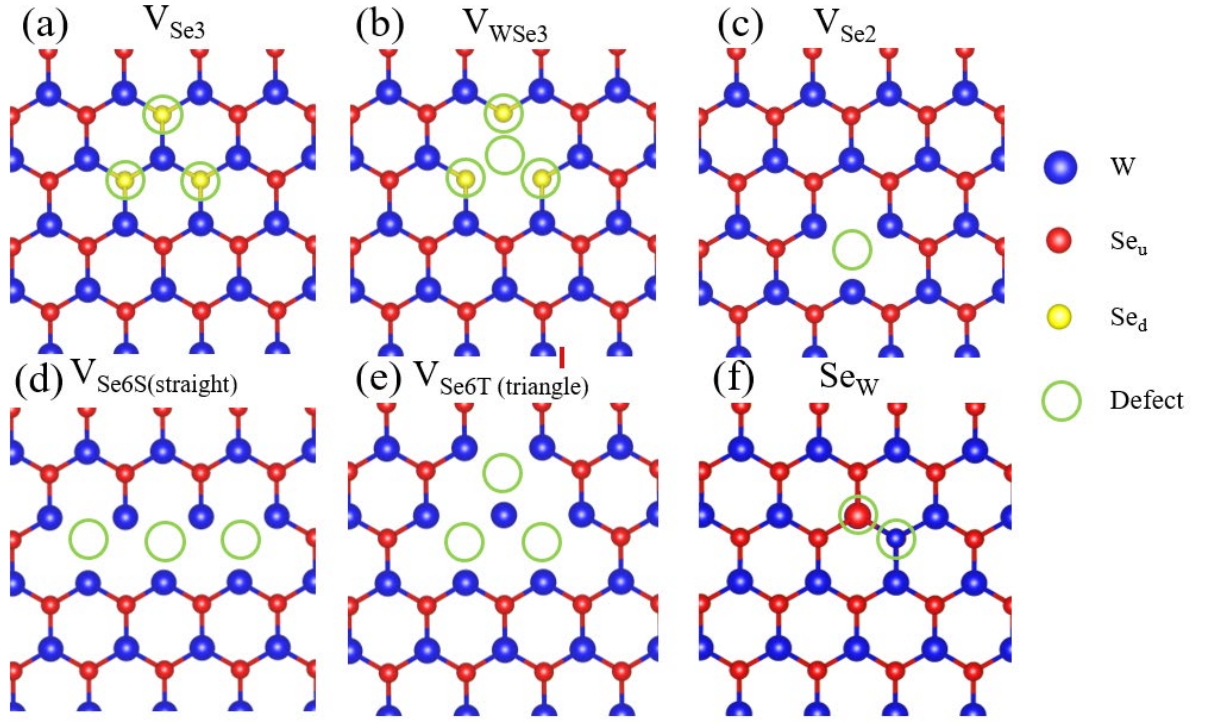


Figure 6. Six kinds of vacancies configuration in single-layer WSe₂: (a) Vacancy complex of three Se atoms, (b) Vacancies of single W and nearby three Se vacancies, (c) Vacancy of double Se atoms (in the same column), (d) Vacancy complex of six missing Se atoms (triangle), (e) Vacancy complex of six missing Se atoms (chain) (f) Anti-site defect of W and Se atom.

We performed MD calculations for the formation energy of various vacancies to compare the stability. The formation energy E_v^f is calculated from the following expression:

$$E_v^f = E_f - \left[\frac{N_0 - N_f}{N_0} \right] * E_i \quad (7)$$

where E_f and E_i represent the final energy after the atoms is removed from the cell, the initial energy of the perfect system, respectively, and N_0 and N_f are the total number of atoms in the cell before and after the atoms being removed.

Table 1. The formation energy of different types of defects in WSe₂.

Defects type	E_v^f (this work)	E_v^f (DFT)[55]	E_v^f (ReaxFF)[55]
V _w	5.71	5.26	5.37
V _{Se}	2.27	2.66	2.34
V _{Se2} (separate)	4.55	-	-
V _{Se2} (in the same column)	4.17	4.82	5.17
V _{Se3}	6.51	-	-
V _{Se6C}	12.95	-	-
V _{Se6T}	13.87	-	-
V _{WSe3}	12.56	10.92	11.71
Se _w	5.49	4.51	4.04

The formation energy of various vacancies investigated in this work are calculated in Table 1. Meanwhile, the formation energies of some type defects calculated by DFT and ReaxFF potential[55] are also listed as comparison. As we can see from the Table 1, a single V_{Se} has the lowest formation energy and the similar results also found in other TMD materials[56], which is also consistent with DFT calculations[34]. Three W atoms relax towards the vacancy site when one Se atom is missing while six dangling Se atom connected to W, which impact the relaxation of these Se atoms. The V_{Se2} defect containing two Se atoms arranged in an apical form has a much lower formation energy than two independent V_{Se}, implying a high probability of aggregation of vacancies.

Chain vacancies are favored over isolated vacancies in higher order vacancies, which is observed by using transmission electron[31]. Comparison of two possible configurations for V_{Se6} : vacancy complex of six Se atoms in triangle form V_{Se6T} and linear chain V_{Se6C} , shows that the latter is more stable by 0.92 eV.

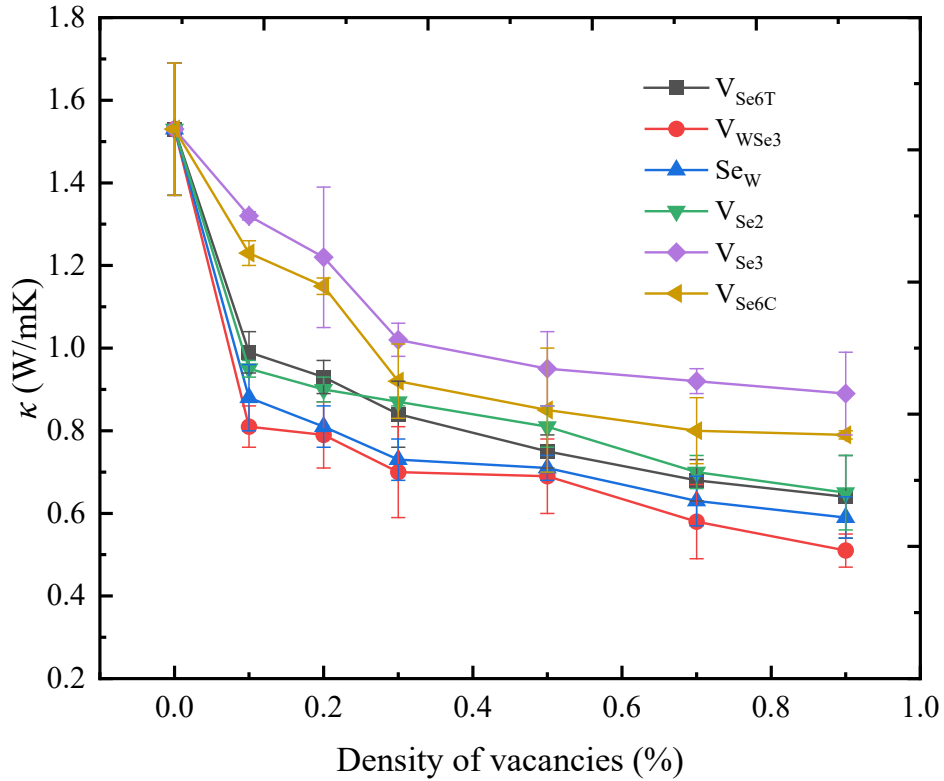


Figure 7. Thermal conductivity of single-layer WSe_2 as a function of the density of vacancies with several types of vacancies (Se_W , V_{WSe3} , V_{Se3} , V_{Se2} , V_{Se6C} , V_{Se6T}).

To investigate the effect of content of each type of defect on single-layer WSe_2 , five independent simulations with randomly produced defective configurations for a specific content are calculated and in a simulation box fixed as 50×10 nm. The averaged thermal conductivity is obtained to ensure a coherent result and reduce the divergency. As seen in Fig. 7, the thermal conductivity of single-layer WSe_2 falls as vacancies are

added and the reduction of the thermal conductivity is influenced by the vacancies type. Because of the increased number of undercoordinated atoms around a vacancy generated by trigonal symmetry (7 and 9 for V_{Se6C} and V_{Se6T} , respectively), the loss of thermal conductivity is greater with V_{Se6T} than V_{Se6C} in the chain vacancies we examined. The anti-site defect Se_w leads to a higher reduction of thermal conductivity due to a strong renormalization of phonons which will be analysed by PDOS later. It is also found in first-principles calculation[34] that the trigonal symmetry in WSe_2 with Se_w defect is broken during structural relaxation process which may be the reason why the thermal conductivity of WSe_2 is highly suppressed to the presence of Se_w defects .

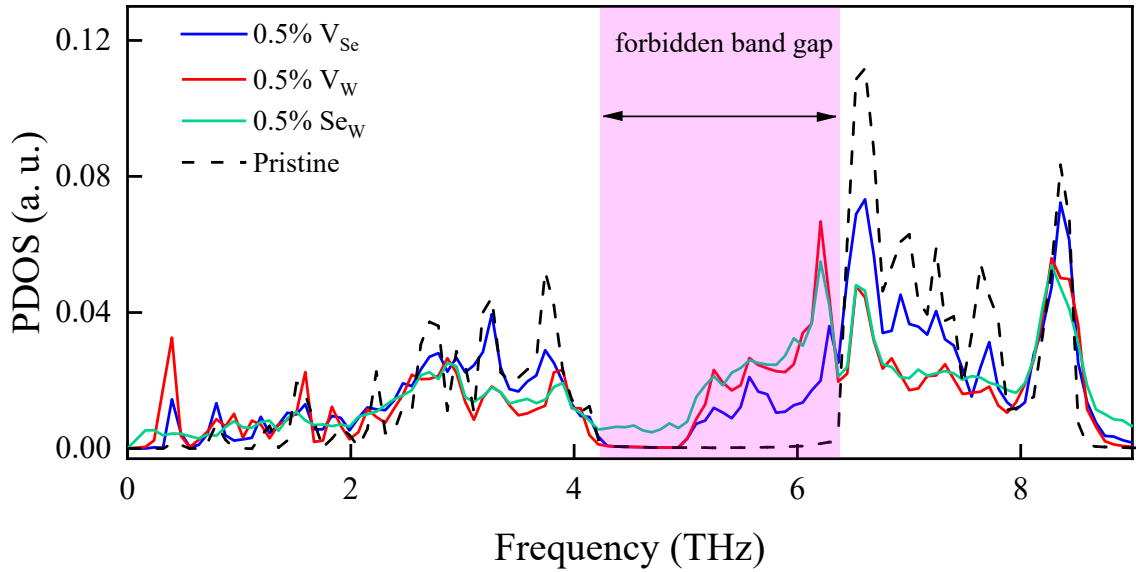


Figure 8. Phonon DOS of single-layer pristine and defective WSe_2 (0.5% V_W , V_{Se} , and Se_w)

We calculate the PDOS of single-layer WSe_2 with 0.5% single V_W , V_{Se} , and Se_w defects respectively to illustrate how the vacancy influences the phonon scattering of

WSe₂. The PDOS would be particularly useful for revealing the alteration of the spectrum of vibrations upon the introduction of bond breaking and formation. In our calculation, a same size of the supercell of WSe₂ is used to allow a direct comparison. We find that all the defects are associated with broadened phonon peaks, especially for those optical branches, while simultaneously reduce the peak intensities in the PDOS. This indicates the bond breaking and reorganization induced by the depletion or replacement of atoms in the defective core. Moreover, the forbidden band gaps between the acoustic and optical branches become narrow in the presence of a defect, compared to that for the pristine WSe₂. Particularly, the gap significantly vanishes in the cases of 0.5% anti-site Se_W defect. These changes reflect the strong potential gradient around the defective core which further explains a decrease in the lifetime of the phonon[57], and accordingly the drop of the thermal conductivity of the WSe₂.

4. SUMMARY

In conclusion, we investigated the effects of width and various single and higher order vacancies on the thermal conductivity of single-layer WSe₂ using EMD method. The thermal conductivity of WSe₂ increases monotonically with size below a critical size of ~5 nm after which the thermal conductivity increases slowly and gradually reaches a constant. It is found that the thermal conductivity of single-layer WSe₂ is significant suppressed by the addition of vacancies defects. The MFP of defective WSe₂ is extrapolated and the decline of MFP is responsible for the reduction of thermal

conductivity. Moreover, the decreased thermal conductivity also depends on vacancy type due to the different missing atom mass and undercoordinated atoms near the vacancies. Higher order defects and the effect on the thermal conductivity are investigated. We found that the impact of the vacancies depends on the missing atom mass, undercoordinated atoms near the vacancies, and the stability of the defective structure. Moreover, the analysis of PDOS of defective WSe₂ reveals that decline in the value of PDOS peaks and shrinkage of forbidden band gaps are accompanied with the reduction of thermal conductivity.

ACKNOWLEDGMENT

This work was supported by the University of Macau (SRG2019-00179-IAPME) and the Science and Technology Development Fund from Macau SAR(FDCT-0163/2019/A3), the Natural Science Foundation of China (Grant 22022309) and Natural Science Foundation of Guangdong Province, China (2021A1515010024). This work was performed in part at the High-Performance Computing Cluster (HPCC) which is supported by Information and Communication Technology Office (ICTO) of the University of Macau.

DATA AVAILABILITY

The data that support the findings of this study are available from the corresponding author upon reasonable request.

CONFLICT OF INTEREST

The authors have no conflicts to disclose.

REFEERNCE

- [1] Chhowalla M, Liu Z and Zhang H 2015 Two-dimensional transition metal dichalcogenide (TMD) nanosheets *Chem. Soc. Rev.* **44** 2584-6
- [2] Lv R, Robinson J A, Schaak R E, Sun D, Sun Y, Mallouk T E and Terrones M 2015 Transition Metal Dichalcogenides and Beyond: Synthesis, Properties, and Applications of Single- and Few-Layer Nanosheets *Acc. Chem. Res.* **48** 56-64
- [3] Chhowalla M, Shin H S, Eda G, Li L-J, Loh K P and Zhang H 2013 The chemistry of two-dimensional layered transition metal dichalcogenide nanosheets *Nat. Chem.* **5** 263-75
- [4] Chen Q, Li L and Peeters 2019 Inner and outer ring states of MoS₂ quantum rings: Energy spectrum, charge and spin currents *J. Appl. Phys.* **125** 244303
- [5] Chen Q, Li L and Peeters 2018 Magnetic field dependence of electronic properties of MoS₂ quantum dots with different edges *Phys. Rev. B* **97** 085437
- [6] Ross J S, Klement P, Jones A M, Ghimire N J, Yan J, Mandrus D, Taniguchi T, Watanabe K, Kitamura K and Yao W 2014 Electrically tunable excitonic light-emitting diodes based on monolayer WSe₂ p-n junctions *Nat. Nanotechnol.* **9** 268-72
- [7] Wang Q H, Kalantar-Zadeh K, Kis A, Coleman J N and Strano M S 2012 Electronics and optoelectronics of two-dimensional transition metal dichalcogenides *Nat. Nanotechnol.* **7** 699-712
- [8] Fan Z-Q, Jiang X-W, Luo J-W, Jiao L-Y, Huang R, Li S-S and Wang L-W 2017 In-plane Schottky-barrier field-effect transistors based on 1T/2H heterojunctions of transition-metal dichalcogenides *Phys. Rev. B* **96** 165402
- [9] Baugher B W, Churchill H O, Yang Y and Jarillo-Herrero P 2014 Optoelectronic devices based on electrically tunable p-n diodes in a monolayer dichalcogenide *Nat. Nanotechnol.* **9** 262-7
- [10] Liu Q, Li J-J, Wu D, Deng X-Q, Zhang Z-H, Fan Z-Q and Chen K-Q 2021 Gate-controlled reversible rectifying behavior investigated in a two-dimensional MoS₂ diode *Phys. Rev. B* **104** 045412
- [11] Pospischil A, Furchi M M and Mueller T 2014 Solar-energy conversion and light emission in an atomic monolayer p-n diode *Nat. Nanotechnol.* **9** 257-61
- [12] Fan Z-Q, Jiang X-W, Chen J and Luo J-W 2018 Improving performances of in-plane transition-metal dichalcogenide Schottky barrier field-effect transistors *ACS Appl. Mater.* **10** 19271-7
- [13] Fan Z-Q, Zhang Z-H and Yang S-Y 2020 High-performance 5.1 nm in-plane Janus WSeTe Schottky barrier field effect transistors *Nanoscale* **12** 21750-6
- [14] Yan X, Chen Q, Li L, Guo H, Peng J and Peeters F 2020 High performance piezotronic spin transistors using molybdenum disulfide nanoribbon *J Nano Energy* **75** 104953
- [15] Ong Z-Y, Zhang G and Zhang Y-W 2021 The role of flexural coupling in heat dissipation from a two-dimensional layered material to its hexagonal boron nitride substrate *2d Mater* **8** 035032
- [16] Yin Y, Li D, Hu Y, Ding G, Zhou H and Zhang G 2020 Phonon stability and phonon transport of graphene-like borophene *Nanotechnology* **31** 315709
- [17] Wang J, Xie F, Cao X-H, An S-C, Zhou W-X, Tang L-M and Chen K-Q 2017 Excellent Thermoelectric Properties in monolayer WSe₂ Nanoribbons due to Ultralow Phonon Thermal Conductivity *Sci. Rep.* **7** 41418
- [18] Chiritescu C, Cahill D G, Nguyen N, Johnson D, Bodapati A, Keblinski P and Zschack 2007 Ultralow thermal conductivity in disordered, layered WSe₂ crystals *Science* **315** 351-3
- [19] Kumar S and Schwingenschlogl 2015 Thermoelectric response of bulk and monolayer MoSe₂ and WSe₂ *Chem. Mater.* **27** 1278-84
- [20] Kim S, Zuo J M, Nguyen N T, Johnson D C and Cahill D G 2008 Structure of layered WSe₂ thin films with ultralow thermal conductivity *J. Mater. Res.* **23** 1064-7
- [21] Zhou W-X and Chen K-Q 2015 First-principles determination of ultralow thermal conductivity of monolayer WSe₂ *Sci. Rep.* **5** 1-8
- [22] Chang Z, Yuan K, Sun Z, Zhang X, Gao Y, Gong X and Tang D 2021 First-principles analysis of phonon thermal transport properties of two-dimensional WS₂/WSe₂ heterostructures *Chin. Phys. B* **30** 034401
- [23] Norouzzadeh P and Singh D J 2017 Thermal conductivity of single-layer WSe₂ by a Stillinger-Weber potential *Nanotechnology* **28** 075708
- [24] Jiang J-W, Park H S and Rabczuk T 2013 Molecular dynamics simulations of single-layer molybdenum disulphide (MoS₂): Stillinger-Weber parametrization, mechanical properties, and thermal conductivity *J. Appl. Phys.* **114** 064307

- [25] Zhou W-X and Chen K-Q 2015 First-Principles Determination of Ultralow Thermal Conductivity of monolayer WSe₂ *Scientific Reports* **5** 15070
- [26] Zheng Y J, Chen Y, Huang Y L, Gogoi P K, Li M-Y, Li L-J, Trevisanutto P E, Wang Q, Pennycook S J and Wee A T 2019 Point defects and localized excitons in 2D WSe₂ *ACS nano* **13** 6050-9
- [27] Jiang J, Xu T, Lu J, Sun L and Ni Z 2019 Defect engineering in 2D materials: precise manipulation and improved functionalities *Research* **2019**
- [28] Wu X and Han Q 2020 Thermal conductivity of defective graphene: an efficient molecular dynamics study based on graphics processing units *Nanotechnology* **31** 215708
- [29] Dongre B, Carrete J, Wen S, Ma J, Li W, Mingo N and Madsen G K 2020 Combined treatment of phonon scattering by electrons and point defects explains the thermal conductivity reduction in highly-doped Si *J. Mater. Chem. A* **8** 1273-8
- [30] Liu X, Gao J, Zhang G, Zhao J and Zhang Y-W 2020 Remarkable Role of Grain Boundaries in the Thermal Transport Properties of Phosphorene *ACS Omega* **5** 17416-22
- [31] Zhao J, Nam H, Ly T H, Yun S J, Kim S, Cho S, Yang H and Lee Y H 2017 Chain vacancies in 2D crystals *Small* **13** 1601930
- [32] Tripathi M, Lee F, Michail A, Anastopoulos D, McHugh J G, Ogilvie S P, Large M J, Graf A A, Lynch P J and Parthenios J 2021 Structural defects modulate electronic and nanomechanical properties of 2D materials *ACS nano* **15** 2520-31
- [33] Xiong Z, Zhong L, Wang H and Li X 2021 Structural Defects, Mechanical Behaviors, and Properties of Two-Dimensional Materials *J Materials* **14** 1192
- [34] Zhang S, Wang C-G, Li M-Y, Huang D, Li L-J, Ji W and Wu S 2017 Defect structure of localized excitons in a WSe₂ monolayer *Phys. Rev. Lett.* **119** 046101
- [35] Wu Z, Luo Z, Shen Y, Zhao W, Wang W, Nan H, Guo X, Sun L, Wang X and You Y 2016 Defects as a factor limiting carrier mobility in WSe₂: A spectroscopic investigation *J Nano Research* **9** 3622-31
- [36] Mavrokefalos A, Nguyen N T, Pettes M T, Johnson D C and Shi L 2007 In-plane thermal conductivity of disordered layered WSe₂ and (W) x (WSe₂) y superlattice films *Appl. Phys* **91** 171912
- [37] Wang J, Xie F, Cao X-H, An S-C, Zhou W-X, Tang L-M and Chen K-Q 2017 Excellent thermoelectric properties in monolayer WSe₂ nanoribbons due to ultralow phonon thermal conductivity *Sci. Rep.* **7** 1-8
- [38] Mortazavi B and Ahzi S 2013 Thermal conductivity and tensile response of defective graphene: A molecular dynamics study *Carbon* **63** 460-70
- [39] Yan Z, Yoon M and Kumar S 2018 Influence of defects and doping on phonon transport properties of monolayer MoSe₂ *J 2D Materials* **5** 031008
- [40] Thompson A P, Aktulga H M, Berger R, Bolintineanu D S, Brown W M, Crozier P S, in 't Veld P J, Kohlmeyer A, Moore S G, Nguyen T D, Shan R, Stevens M J, Tranchida J, Trott C and Plimpton S J 2022 LAMMPS - a flexible simulation tool for particle-based materials modeling at the atomic, meso, and continuum scales *Comput. Phys. Commun.* **271** 108171
- [41] Huang W, Luo X, Gan C K, Quek S Y and Liang G 2014 Theoretical study of thermoelectric properties of few-layer MoS₂ and WSe₂ *Phys. Chem* **16** 10866-74
- [42] Chan H, Sasikumar K, Srinivasan S, Cherukara M, Narayanan B and Sankaranarayanan S K R S 2019 Machine learning a bond order potential model to study thermal transport in WSe₂ nanostructures *Nanoscale* **11** 10381-92
- [43] Chan H, Sasikumar K, Srinivasan S, Cherukara M, Narayanan B and Sankaranarayanan S K 2019 Machine learning a bond order potential model to study thermal transport in WSe₂ nanostructures *Nanoscale* **11** 10381-92
- [44] Green M S 1954 Markoff random processes and the statistical mechanics of time - dependent phenomena. II. Irreversible processes in fluids *J. Chem. Phys.* **22** 398-413
- [45] Wang B, Yan X, Yan H and Cai Y 2022 Size and stoichiometric dependence of thermal conductivities of In_xGa_{1-x}N: A molecular dynamics study *Comput. Mater. Sci.* **207** 111321
- [46] Kubo R 1957 Statistical-mechanical theory of irreversible processes. I. General theory and simple applications to magnetic and conduction problems *J. Phys. Soc. Japan* **12** 570-86
- [47] Zhou X W, Aubry S, Jones R E, Greenstein A and Schelling P K 2009 Towards more accurate molecular dynamics calculation of thermal conductivity: Case study of GaN bulk crystals *Phys. Rev. B* **79** 115201
- [48] Polanco C A, Pandey T, Berlijn T and Lindsay L 2020 Defect-limited thermal conductivity in MoS₂ *Phys. Rev. Mater* **4** 014004
- [49] Yan Z, Yoon M and Kumar S 2018 Influence of defects and doping on phonon transport properties of monolayer MoSe₂ *2d Mater* **5** 031008
- [50] Chen D, Chen H, Hu S, Guo H, Sharshir S W, An M, Ma W and Zhang X 2020 Influence of atomic-scale defect on thermal conductivity of single-layer MoS₂ sheet *J. Alloys Compd.* **831** 154875

- [51] Poetzsch R H and Böttger H 1994 Interplay of disorder and anharmonicity in heat conduction: molecular-dynamics study *Phys. Rev. B* **50** 15757
- [52] Matthiessen A and Vogt C 1864 IV. On the influence of temperature on the electric conducting-power of alloys *Philosophical Transactions of the Royal Society of London* 167-200
- [53] Xie G, Shen Y, Wei X, Yang L, Xiao H, Zhong J and Zhang G 2014 A bond-order theory on the phonon scattering by vacancies in two-dimensional materials *Sci. Rep.* **4** 1-6
- [54] Klemens P G and Pedraza D F 1994 Thermal conductivity of graphite in the basal plane *Carbon* **32** 735-41
- [55] Nayir N, Wang Y, Shabnam S, Hickey D R, Miao L, Zhang X, Bachu S, Alem N, Redwing J, Crespi V H and van Duin A C T 2020 Modeling for Structural Engineering and Synthesis of Two-Dimensional WSe₂ Using a Newly Developed ReaxFF Reactive Force Field *J. Phys. Chem. C* . **124** 28285-97
- [56] Haldar S, Vovusha H, Yadav M K, Eriksson O and Sanyal B 2015 Systematic study of structural, electronic, and optical properties of atomic-scale defects in the two-dimensional transition metal dichalcogenides *Phys. Rev. B* **92** 235408
- [57] Turney J, Landry E, McGaughey A and Amon C 2009 Predicting phonon properties and thermal conductivity from anharmonic lattice dynamics calculations and molecular dynamics simulations *Phys. Rev. B* **79** 064301